Adsorption on Carbon Nanotubes Studied Using Polarization-Modulated Infrared Reflection−Absorption Spectroscopy

V. M. Bermudez*

Electronics Science and Technology Division, Naval Research Laboratory, Washington, D.C. 20375-5347

Received: February 16, 2005; In Final Form: April 4, 2005

Single-wall carbon nanotubes (SWNTs), deposited onto an Al substrate from a liquid suspension, have been cleaned by annealing in ultrahigh vacuum. The effects of exposing the sample in situ to atomic H (or D) and/or to dimethyl methylphosphonate [DMMP, $(CH_3O)_2(CH_3)P{=}O$] were then studied using polarization-modulated infrared reflection−absorption spectroscopy. Atomic H reacts preferentially near strained or defective regions in the nanotube wall to produce a spectrum consistent with alkane-like species ($>CH_2$ and $-CH_3$). Only a small fraction of the $>C{=}C<$ sites in the nanotube wall react with H, and there is no clear evidence for monohydride $>C(H)-C(H)<$ species. For DMMP, data were obtained under steady-state conditions in reagent pressures in excess of half the room-temperature vapor pressure. Adsorption occurs via the P═O group with a coverage that depends on the ambient pressure. Varying the DMMP coverage by changing the pressure causes changes in the spectrum that can be related to the strength of the DMMP/SWNT interaction. Preadsorbed H is seen to have little or no effect on the subsequent adsorption of DMMP. For DMMP, the molecular features are superimposed on a broad, smoothly varying background that can be related to adsorption-induced changes in the Drude parameters characterizing the SWNT free-carrier density and scattering lifetime.

1. Introduction

The chemistry of single-wall carbon nanotubes (SWNTs) has been a subject of interest for several years. (For recent reviews, see refs 1−3.) Much of this work has used vibrational spectroscopy (either infrared (IR) or Raman) as the most suitable technique for identifying functional groups and has focused on samples prepared in liquid media and handled in ambient air. The high surface-to-volume ratio of even multiwall nanotubes makes chemical phenomena intrinsically surface-related and suggests the value of working with well-characterized samples under controlled conditions. Furthermore, contamination by atmospheric species (e.g., H_2O and O_2) is known[4−8] to be important in the electronic properties of SWNTs. Despite this, few studies of SWNT chemistry have combined vibrational spectroscopy with any form of surface analysis, such as X-ray photoemission or Auger electron spectroscopy (XPS or AES). The purpose of the present work is to evaluate a method for performing IR studies of adsorption on SWNTs that is also fully compatible with the use of such electron spectroscopies.

Designing an experiment that permits both IR and electron-spectroscopic studies of SWNTs presents certain difficulties. The standard approach to obtaining IR data for SWNTs is to deposit samples on an IR-transmitting material such as KBr or CaF_2. However, all such halides are extremely susceptible to damage (i.e., halogen desorption) by electron impact which results in a defective surface layer[9] capable of reacting with the SWNTs and/or the reagent being studied. Oxides such as SiO_2 or Al_2O_3, although somewhat less easily damaged by electron impact (especially when free of surface −OH groups[10]), have unfavorable IR transmission properties for substrates of practical thickness (∼0.3 mm or more). In addition, insulating substrates (even those less susceptible to damage, such as ZnSe) present the problem of charging during electron-beam irradiation or photoelectron emission.

Three possible solutions were initially considered here: (a) free-standing SWNT films[11] sandwiched between layers of W mesh for support and for resistive heating, (b) films deposited on semiconductor wafers (Si or Ge), and (c) films deposited on a metallic substrate. Methods a and b involve IR transmission measurements at near-normal incidence. Method c employs reflectance at a high (∼82°) angle of incidence with respect to the surface normal and is thus termed "IR reflection−absorption spectroscopy" (IRRAS). Preliminary results for method a showed that it was difficult to prepare a sample thin enough for good mid-IR transmission that was also free of pinholes and sufficiently robust to allow handling and mounting. However, a variation of this method, in which SWNTs are deposited from a liquid suspension onto a fine W mesh, has been used elsewhere.[12,13] Method b is a workable solution; however, many reagents of interest will chemisorb readily at room temperature on Si, Ge, and their oxides as well as on SWNTs which complicates the interpretation of spectroscopic data. There is also the potential problem of reaction (e.g., SiC formation[14]) during cleaning of the SWNTs by annealing in ultrahigh vacuum (UHV).

The present work has made use of method c, which provides a number of advantages over other methods and which has already been used[15] to facilitate the recording of AES and XPS data for SWNT samples. For a thin dielectric layer (∼100 nm thick or less) on a metallic substrate, which is termed a "buried metal layer" (BML) structure, the mid-IR optical properties are dominated by those of the metal (e.g., refs 16 and 17 and references therein). Specifically, the electric field intensity at the surface is negligibly small except in p-polarization and at a high angle of incidence. This combination of a high electric field intensity *and* a high angle of incidence is what makes IRRAS sensitive to sub-monolayer coverages of adsorbates on

* Phone: +1-202-767-6728. Fax: +1-202-767-1165. E-mail: bermudez@estd.nrl.navy.mil.

10.1021/jp0508150
Published on Web 04/30/2005

metals.[18] For nonmetals, on the other hand, the surface electric field intensity maximizes at a smaller value and at a smaller angle of incidence than for a metal. The BML approach has been used by many groups[19−24] to enhance the IRRAS sensitivity to adsorbates on nonmetallic surfaces over what can be attained in external reflection measurements on the same materials in bulk form. The thickness of the nonmetallic layer typically employed in a BML experiment is such that the layer is "optically thin but chemically thick". This means that the mid-IR optical properties are essentially those of the metal, but the chemical response to adsorbates is that of the nonmetallic material of interest.

The polarization properties described above define the so-called "metal-surface IRRAS selection rule"[18] which dictates that only adsorbate vibrational modes with a finite component of the dynamic dipole moment along the surface normal are detectable, and then only in p-polarization and at a high angle of incidence. The s-polarized IR radiation does not couple to the vibrational modes of adsorbates on metals or on BML substrates because the electric field vanishes at the surface. One can make use of this effect by employing polarization modulation (PM) to measure the quantity $\Delta R/R \equiv (R_s - R_p)/(R_s + R_p)$, where R_s (R_p) is the s (p)-polarized reflectance. This offers two distinct advantages over a transmission measurement, although at the expense of an increased experimental complexity. First, weak adsorbate absorptions (which appear only in p-polarization) can be seen in the presence of much stronger but isotropic gas-phase absorptions. This has been exploited in a number of in situ studies[25−29] of surface reactions at elevated reagent pressures and is expected to be useful in observing SWNT surface chemistry under practical conditions. Many species of interest adsorb only weakly on SWNTs, and maintaining a sufficiently high coverage at room temperature requires experiments to be performed under a finite steady-state reagent pressure. Second, R_s is unaffected by the adsorbate and thus serves as a reference signal, making the experiment in effect a double-beam measurement even though there is physically only one IR beam. Hence, the PM experiment is relatively immune to the drift and instrumental instabilities that affect true single-beam IRRAS.

The adsorbates considered here are atomic H (and D) and dimethyl methylphosphonate [DMMP, $(CH_3O)_2(CH_3)P{=}O$] which are of interest for specific reasons. Adsorption of H has been found[30−32] to have the potentially useful effect of converting SWNTs from metallic to semiconducting, and the vibrational spectrum of adsorbed H can be a useful probe of surface structure (e.g., for semiconductors[33]). Sensors based on SWNTs have been demonstrated for a number of gases including DMMP,[34] which is of interest as a simulant for pesticides and for chemical warfare nerve agents. However, the surface chemistry involved in adsorption of DMMP on SWNTs has not been studied in detail. The combined use of the BML and PM-IRRAS approaches, described above, permits the detection of these species on SWNTs with high sensitivity and under "high" ambient pressures. Although AES and XPS data were not obtained in the present study, due to instrumental limitations, the sample configuration is completely compatible with such measurements.[15]

2. Experimental Details

2.1. Infrared Measurements. The PM Fourier transform infrared (FTIR) apparatus and measurement techniques have been described in detail previously,[26] although some improvements have been incorporated since the original work. The UHV chamber has also been described previously.[26] The spectrometer is now a Nicolet 870 which permits simultaneous recording of both the unmodulated (R) and polarization-modulated (ΔR) interferograms. In addition to halving the data acquisition time, this eliminates instabilities associated with recording the two interferograms sequentially. The "narrow-band" $Hg_xCd_{1-x}Te$ (MCT) detector now has a preamplifier with built-in compensation for nonlinear response.[35,36] These modifications greatly improve the cancellation of strong gas-phase absorptions in the individual single-beam spectra. As discussed in ref 26, $\Delta R/R$ is related to S, the measured signal after intensity calibration, by $\Delta R/R = S/[1 \pm J_0(A)(1 - S)]$, where $J_0(A)$ is the zeroth-order Bessel function of the phase modulation amplitude A. The sign depends on the azimuthal angles of the polarizer and modulator relative to the surface normal. The correct sign, as well as the value of A (which varies with the IR wavelength), can easily be determined (see below) from the overall shape of the intensity-calibration spectrum. Since A is known at any point in the spectrum, $J_0(A)$ can be computed and used to obtain $\Delta R/R$ from the measured signal. This procedure, rather than the approximation described in ref 26, was used to include the effect of the dependence of $J_0(A)$ on photon energy. This correction, which is often neglected in PM-IRRAS, can significantly affect relative intensities across the spectrum. The difference between the corrected $\Delta R/R$ spectra thus obtained before and after gas exposure then gives the final quantity of interest, $\delta(\Delta R/R)$, which is the change in the spectrum due to the adsorbate. Given the definition of $\delta(\Delta R/R)$, features in the spectrum arising from absorption caused by the adsorbate will be "positive" (i.e., upward-pointing) and those due to absorptions that are removed by the adsorbate will be "negative" (i.e., downward-pointing).

The PM-IRRAS data were obtained at 8 cm^{-1} resolution, typically by averaging 2000 scans in 17 min. Triangle apodization and 4-fold zero-filling were applied to the interferograms before Fourier transformation. The phase modulation was set to give half-wave amplitude (i.e., $A = \pi$) at 2600 cm^{-1} which can be checked[26] by comparing the shapes of the observed and calculated intensity-calibration spectra, given by $cJ_2(A)/(1 \pm J_0(A))$, where c is a constant independent of photon energy and $J_2(A)$ is the second-order Bessel function of A. The variation of A with photon energy, which depends on the choice of the half-wave point, determines the energy dependence of the experimental sensitivity.[26] Data were obtained in the 4000−700 cm^{-1} range, with the lower limit being fixed by the transmission cutoff of the ZnSe polarization modulator and by the detector response.

2.2. Sample and Reagents. The SWNT sample was deposited by spraying a suspension in *N*,*N*-dimethylformamide (DMF, ∼5 mg/L) from an airbrush onto the substrate at about 200 °C. The suspension was prepared by ultrasonic agitation of a concentrated mixture (∼50 mg/L) of SWNT bundles in DMF followed by dilution. The SWNT stock was single-walled HiPco material obtained from Carbon Nanotechnologies Inc. (CNI) with a stated purity of about 96% and was used without further processing. The SWNT film appeared to the unaided eye as a faint and uniform dull black haze on the substrate. The substrate was an electrolytically polished Al block. A second, nominally identical Al block with no SWNT layer was used as a reference, and this block included a small hole in which a chromel−alumel thermocouple was buried for temperature measurement. A manipulator allowed positioning of one block or the other in the light path. The samples were mounted in an UHV chamber with a base pressure of $< 2 \times 10^{-10}$ Torr after ∼18 h of baking at about 140 °C. It has been found[37] that SWNTs do not react with Al at temperatures below about 700 °C, which is above

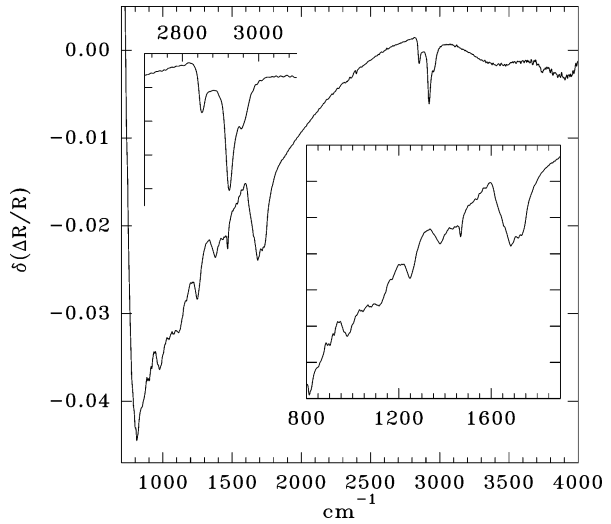

Figure 1. PM-IRRAS data showing the effect of annealing at 307 °C in a vacuum on the as-inserted SWNT/Al sample. The plot shows the $\Delta R/R$ spectrum of the annealed sample after subtraction of the spectrum before thermal treatment, and the negative (downward-pointing) peaks indicate the desorption of surface species. The insets show parts of the spectrum in more detail. The very weak structure near 2400 cm^{-1}, seen in this spectrum and in others, is an artifact resulting from the signal-processing electronics.

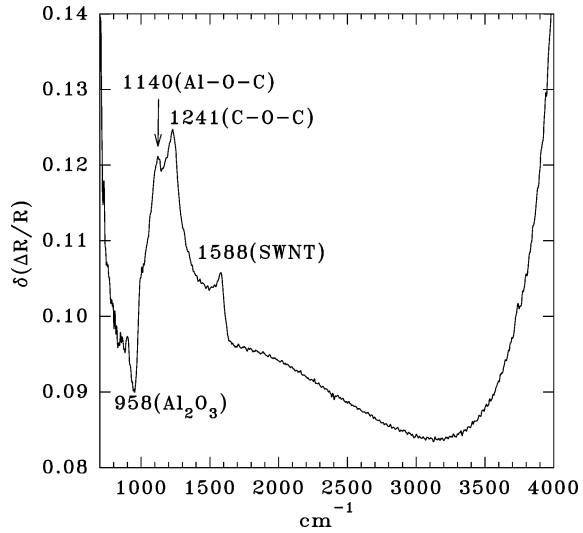

Figure 2. $\Delta R/R$ spectrum of the 520 °C-annealed SWNT/Al sample after subtraction of the spectrum of a bare Al substrate subjected to the same annealing. The positive (upward-pointing) features indicate absorption associated with the SWNTs. The peak assignments are discussed in the text.

the Al melting point of 660 °C. Also, no degradation of the sample (e.g., a change in chemisorption behavior) was noted after many annealing treatments up to 520 °C (see below). The thermally stable native oxide on the Al surface probably impeded any extensive carbide formation.

Exposure to H or D atoms was done by back-filling the chamber with nominally 99.995% pure H_2 or 99.65% pure D_2 gas through a leak valve with a W filament resistively heated to ∼1700−1800 °C at a distance of about 5 cm from the sample. The H_2 cracking efficiency on W at this temperature[38] is ∼2.5%. The gas was pumped continuously by a cryopump while maintaining a pressure of $\sim 5 \times 10^{-6}$ Torr (H_2) or $\sim 4 \times 10^{-5}$ Torr (D_2), based on uncorrected cold-cathode ionization gauge readings. The H_2 and D_2 exposures are given in Langmuirs (L) where $1\ L = 1 \times 10^{-6}$ Torr•s. The purity of the gas was checked using a quadrupole mass spectrometer in the UHV chamber. The sample was biased at −11 V to repel low-energy electrons from the hot filament, and a positive voltage drop (∼8 V) was maintained across the filament during operation to impede electron emission. The sample temperature typically rose to ∼60 °C due to radiative heating by the filament.

The DMMP was stored in a glass bulb and degassed by repeated freeze−pump−thaw cycles, with freezing in liquid N_2. Exposures were done by static back-filling of the chamber through a leak valve. The purity was checked using an IR transmission spectrum of the gas in the chamber during an experiment. This was obtained from the ratio of the unmodulated (R) single-beam spectra recorded before and after admitting the gas and was compared to a standard reference spectrum.[39]

3. Results and Discussion

3.1. In Situ Carbon Nanotube Cleaning. Previous IR studies[40,41] have shown that SWNTs contain adsorbed O in the form of C−OH and C═O species until heated in UHV to at least 450 °C. Other work[4,13] indicates that a much higher temperature is needed to remove completely all traces of O. Figure 1 shows PM-IRRAS data illustrating the effect of annealing the "as-inserted" sample to 307 °C in a vacuum of ∼5×10^{-9} Torr in the unbaked UHV chamber (see above). The spectrum was obtained by recording $\Delta R/R$ for the as-inserted sample and subtracting it from $\Delta R/R$ recorded after annealing and is intended to indicate the range of species that desorb from an otherwise-untreated sample under moderate in vacuo annealing. Here, the negative peaks in the $\delta(\Delta R/R)$ difference spectrum show the removal of surface species by the annealing process. The desorption of alkane-like hydrocarbon contaminants is indicated by the C−H stretching modes at 2851, 2923, and 2955 cm^{-1}. Some of the other features in Figure 1 have been discussed elsewhere.[13,40,41] The broad band at ∼3450 cm^{-1} indicates the loss of H-bonded −OH groups and/or physisorbed H_2O. The structure in the 1680−1735 cm^{-1} range has been assigned to the loss of various carbonyl (>C═O) species. The other features are assumed to be associated with the removal of adsorbed hydrocarbons; however, no attempt at a complete assignment has been made. It is noted that temperature-programmed desorption studies[42] have suggested that the pyrolysis of O-containing sites leaves the nanotube wall in a strained and more reactive state than a pristine SWNT.

Figure 2 shows the spectrum of the SWNT sample after heating in UHV to 520 °C, *referenced to that of the bare Al substrate*. This is the maximum annealing temperature used in the present work and was the typical treatment prior to adsorption studies. Here, $\delta(\Delta R/R)$ was obtained by subtracting $\Delta R/R$ for the bare Al reference sample (see above), which was annealed identically, from that of the SWNT/Al sample. The spectrum cannot be directly related in any simple way to the "true" IR spectrum of the SWNTs themselves for two reasons. First, the subtraction used to obtain $\delta(\Delta R/R)$ involves the assumption that optical absorption in the surface layer (the SWNTs) has a small and strictly additive effect on the reflectance of the bare substrate (Al). While this is valid for the weakly absorbing, sub-monolayer adsorbate layers of interest here,[18] it is not true for the SWNT layer itself. Second, the IR polarization vector within the SWNT film makes an angle with respect to the surface normal which is determined by the angle of incidence and by refraction at the vacuum/SWNT interface. The SWNT film, consisting of a network of tubes "lying flat", has anisotropic optical properties[43] that depend on this angle. The value of Figure 2 is in identifying chemical species

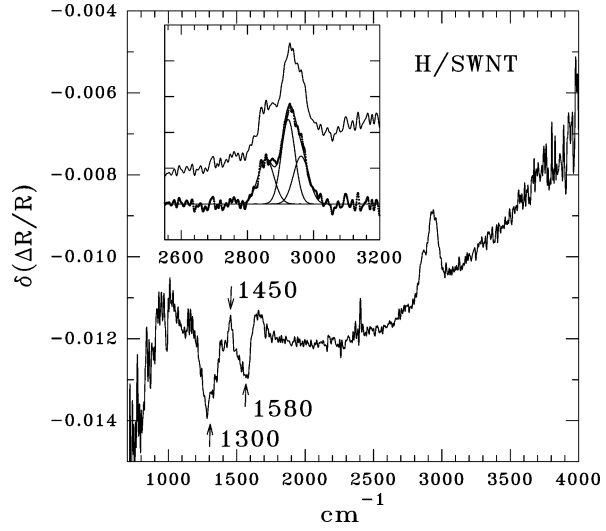

Figure 3. PM-IRRAS data for a SWNT/Al sample exposed to H atoms. The inset shows the C−H stretching region in detail together with a least-squares fit with three Gaussians and a quartic polynomial background. The points show the data after subtraction of the fitted background, and the lines show the three components and the total fit. The upper trace in the inset shows the raw data. Note the difference in the scale of $\delta(\Delta R/R)$ versus Figures 1 and 2.

remaining after a maximum annealing treatment in UHV. For example, a species that is completely unaffected by annealing would not appear in the $\delta(\Delta R/R)$ difference spectrum in Figure 1 but would be seen in Figure 2.

The feature at 1588 cm^{-1} is assigned to the SWNT phonon observed very near this energy in IR[40,41,44] and Raman[45] spectra. No indication of the hydrocarbon or carbonyl absorptions, noted above, is seen for the annealed sample. The band at 1241 cm^{-1} is assigned to the C−O stretching[40,41] associated with C−O−C groups in the nanotube wall. Previous work[13,15,40,41] indicates that annealing in excess of 700 °C is needed to eliminate these species. The peak at 1140 cm^{-1} is assigned to Al−O−C groups formed by C atoms in direct contact with the oxidized Al surface. This is based on the Al−O−CH_3 stretching frequency[46] of 1091 cm^{-1} for CH_3O− on Al_2O_3 and is consistent with the presence of a negative feature at 958 cm^{-1}, the longitudinal-optic phonon frequency[47] for a very thin Al_2O_3 film on Al, which indicates the loss or modification of oxide on the Al surface. This feature did not appear strongly in the spectrum until the SWNT/Al interface had been annealed above ∼400 °C. Previous IRRAS results[48] (without PM) for SWNTs deposited on electrolytically polished Al (without subsequent annealing) also show a band at about 1200 cm^{-1} which was assigned to a disorder-induced SWNT mode. It is noted that the electric field intensity in a BML structure is largest at the metal surface which will enhance the IRRAS intensity for species directly adsorbed on the metal versus farther away in the SWNT layer.

3.2. Hydrogen. No H-related absorptions were observed, for SWNT samples cleaned as described above, in an ambient of $\sim 10^{-4}$ Torr of H_2 in the absence of a hot W filament. Molecular H_2, which can be seen in Raman spectra[49] of SWNTs in a high pressure of H_2, would be difficult to detect in the IR, even for molecules in a non-centrosymmetric environment within a SWNT. In any case, the present experimental sensitivity is poor in the region of the H_2 mode (∼4150 cm^{-1}). Figure 3 shows data for H-atom exposure. An H_2 exposure of $\sim 2 \times 10^4$ L, under the conditions described above, was sufficient to reach saturation in that further exposure led to no significant change in the spectrum. None of the features in Figure 3 were seen when exposing the bare Al reference sample to H atoms. It is also noted that the peak intensities in Figure 3 are small compared to those in Figures 1 and 2. A limited study (not shown) was performed of the effect on the H-exposed sample of annealing in UHV. Up to 150 °C, little or no change was seen other than a sharpening of the C−H stretching absorptions. A 300 °C anneal caused a loss of about two-thirds of the C−H intensity.

Least-squares fits in the C−H stretching region, using a sum of Gaussians and a quartic polynomial background function, were done to define more clearly the peak positions and relative intensities. A two-component fit reveals peaks at 2853 and 2935 cm^{-1} with a full width at half-maximum (fwhm) of 49 and 75 cm^{-1}, respectively. The data could also be fitted with a sum of three Gaussians but with little or no improvement in the quality of the fit, as measured by the sum of (fit-data)^2 over all points. The three-component fit (shown in Figure 3) gives peaks at 2856, 2923, and 2962 cm^{-1} with a fwhm of 57, 49, and 55 cm^{-1}, respectively. There is no statistical basis for favoring the three-component fit. However, the higher-energy band does appear (reproducibly, for all experiments) to consist of a peak with a shoulder on the high-energy side. This fact, and the similarity of all fwhm's for the three-component fit, suggests that it is the correct model. These widths are much greater than the instrumental resolution of 8 cm^{-1} and indicate a high degree of inhomogeneous broadening. The Lorentzian width of a C−H stretching mode in this case is expected[50] to be negligible (∼1 cm^{-1}). An interpretation of the C−H stretching modes will be presented after additional data are examined.

Figure 3 shows a negative peak at about 1580 cm^{-1} which indicates the removal of >C═C< groups by H adsorption. A comparison of the intensity of the >C═C< peak in Figures 2 and 3 indicates that H adsorption under the present conditions removes only a small fraction (roughly 10%) of such sites. Figure 3 shows one, and perhaps two, other features. One is the negative peak at ∼1300 cm^{-1}. A peak at about this energy is typically observed in SWNT Raman spectra[51] (where it is termed the "D-band") and assigned to regions of disorder, defects,[52] and/or sp^3-hybridized sites.[53] In IR transmission data,[13,40,41] an ill-defined structure in the 1300−1500 cm^{-1} range is typically observed but not assigned. If the 1300 cm^{-1} peak is, in fact, associated with strain or defects of some kind, then the data are consistent with these being reactive sites. The elimination of the Raman D-band by thermal oxidation has been reported,[54] and previous theoretical work[55,56] indicates that adsorption of H should be enhanced near regions of strain in nanotube walls. In the region between the negative 1300 and 1580 cm^{-1} peaks, there is a suggestion of a positive peak at about 1450 cm^{-1}, the expected energy of a C−H bending mode. For example, on the hydrogenated C(100)-(2 × 1) (diamond) surface, a C−H bending mode of the >C(H)−C(H)< group is found at 183 meV (1476 cm^{-1}) in high-resolution electron energy loss spectra.[57]

For H/SWNT, regardless of whether a C−H bending mode can be detected in the PM-IRRAS data, the fact remains that it is expected to occur in the vicinity of 1450 cm^{-1}. Hence, the first overtone (∼2900 cm^{-1}, neglecting anharmonicity) falls in the range of the C−H stretching fundamentals, and attention must then be paid to the possibility of Fermi resonance. In this process (see, e.g., ref 58), an overtone of a lower-energy mode is accidentally degenerate with a higher-energy fundamental of the same symmetry. Mixing of the overtone and fundamental, via anharmonic coupling, leads to "intensity borrowing" by the normally weak overtone absorption and to a "repulsion" or "avoided crossing" which shifts the two components away from

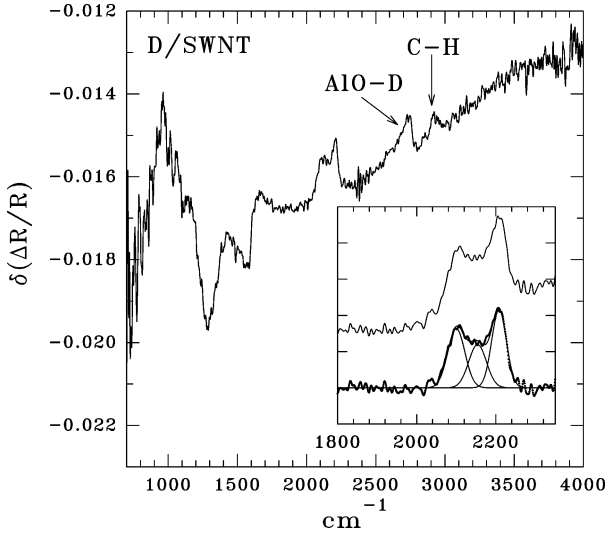

Figure 4. Similar to Figure 3 but showing the results for adsorption of D atoms. The AlO−D stretching mode, due to D adsorption on the substrate oxide, is indicated.

each other and from their unperturbed positions. If such an effect were important here, then one of the modes identified above as "C−H stretching" might in reality be the overtone of a C−H bending mode.

To test this possibility, and also to help clarify the low-energy end of the spectrum by shifting any bending mode to below the 1200−1600 cm^{-1} range, the experiment was repeated with D_2 instead of H_2. For the diamond (100)-(2 × 1)D surface,[59] for example, the overtone of the C−D bend at 1054 cm^{-1} is sufficiently far from the C−D stretching fundamental at 2181 cm^{-1} that Fermi resonance should be precluded. In the present case of SWNTs, observation of three "C−H stretches" but only two C−D stretches would signal a Fermi resonance for the former.

Figure 4 shows the D-atom data in the same form as the H-atom data in Figure 3. The C−D stretching region (∼2050−2250 cm^{-1}) cannot be fitted well with only two Gaussians, but a three-component fit in the C−D region gives peak energies (fwhm's) of 2100 (51), 2153 (53), and 2208 (44) cm^{-1}. The fwhm values are close to the corresponding C−H widths given above, and the ν_{CH}/ν_{CD} ratios are in the range 1.34−1.36, as expected from results[60] for *n*-alkyl chains. The observation of three C−D modes indicates that any effect of Fermi resonance on the C−H stretching region is negligible at the level of the sensitivity and resolution of the present data, possibly as a result of there being only a weak anharmonic coupling to the bending overtone. Furthermore, the fact that ν_{CH}/ν_{CD} lies in the expected range for all three modes argues against the Fermi resonance repulsion effect noted above which would have yielded an anomalous value for one or more ν_{CH}/ν_{CD} ratios. However, it is unclear why the relative intensities are different in the C−H and C−D spectra.

Figure 4 also shows a weak feature in the C−H stretching range, due to H_2 contamination in the D_2, and a peak at ∼2728 cm^{-1} with some evidence of a shoulder on the low-energy side. This feature is assigned to the AlO−D stretch[61] due to D adsorption on the oxidized Al substrate, and the shoulder may result from hydrogen bonding between adjacent AlOD sites. The absence of a similar feature in Figure 3 for H adsorption (at 3745 cm^{-1}, ref 61) results from the poor sensitivity at the extreme high-energy end of the spectrum. Repeating the H/SWNT experiment, after adjusting the phase modulation amplitude (see above) to increase sensitivity in this region, revealed a broad band in the 3600−3700 cm^{-1} range consistent with H-bonded −OH groups on Al_2O_3 (ref 62). There is, however, no indication of a CO−D stretching mode in the 2400−2500 cm^{-1} range in Figure 4 which would indicate attack by D atoms on C−O−C groups in the nanotube wall. Figure 4 also shows the same negative peaks, at about 1300 and 1580 cm^{-1}, as do the H-atom data in Figure 3. However, the apparent positive peak at 1450 cm^{-1} (Figure 3) due to C−H bending has been shifted to lower energy by D substitution. The C−D bending mode is expected to fall in the 950−1050 cm^{-1} range, but the signal-to-noise ratio in the present data is not sufficient to permit a clear identification of this mode.

We now proceed to an interpretation of the results given above. A >C(H)−C(H)< structure is predicted theoretically[31,32,63−66] to be the result of adsorbing H atoms on a "perfect" SWNT. This species exhibits two C−H stretching modes, namely, symmetric (ν_s) and asymmetric (ν_a). For the hydrogenated C(100)-(2 × 1) surface,[67] only one of the two modes of this "monohydride" structure is sufficiently intense to be detected in a multiple internal reflection experiment and is found at 2897 cm^{-1}. It is also seen[67] to have an annealing dependence different from that of $>CH_2$ modes, which are also found at 2854 and 2921 cm^{-1}. None of the H/SWNT modes seen here are sufficiently close in energy to 2897 cm^{-1} to be assigned with confidence to >C(H)−C(H)<. On the other hand, the energies are all close to those typically observed[60,68] for *n*-alkanes. For these species, $\nu_a(>CH_2)$ and $\nu_s(>CH_2)$ fall near 2920 and 2851 cm^{-1}, respectively, and $\nu_a(-CH_3)$ occurs near 2957 cm^{-1}. The $\nu_a(-CH_3)$ mode consists of in-plane and out-of-plane components which are ∼10 cm^{-1} apart and would not be resolvable in the present data. The $\nu_s(-CH_3)$ mode undergoes Fermi resonance with the overtone of the $\delta_a(-CH_3)$ asymmetric deformation, and this effect produces absorptions at about 2937 and 2878 cm^{-1}. In samples with randomly oriented alkyl chains, the intensity of either of these features is less than that of the $\nu_a(-CH_3)$ mode near 2957 cm^{-1}.

Applying these results to the present data then suggests a model in which H reacts preferentially[55,56] at or near defective or strained sites, causing a reduction in intensity in the 1300 cm^{-1} mode, as well as a loss of some >C═C< sites (1580 cm^{-1}), to produce alkyl-like $-(CH_2)_nCH_3$ or $-C(H_2)-C(H_2)-$ species. Such a process implies an opening of holes in the nanotube wall. Similar structures have been suggested for nanotubes grown by radio frequency plasma-enhanced[69] or electron cyclotron resonance chemical vapor deposition,[70] for which C−H spectra similar to those obtained here were observed. There is no clear spectroscopic evidence in the present data for the formation of a high concentration of >C(H)−C(H)< sites. Perhaps this mode of adsorption is inhibited by the presence of C−O−C groups in the nanotube wall, which has not to our knowledge been considered in theoretical discussions.

3.3. DMMP. The adsorption of DMMP on nonmetals, primarily on oxides,[71−76] has been studied extensively due to its importance as a simulant for toxic nerve agents and pesticides. The interaction of DMMP with activated carbon[77] and with alkanethiolate self-assembled monolayers (SAMs) on Au[78] has also been investigated. Activated carbon is found[77] to catalyze the decomposition of DMMP at elevated temperatures, and the SAM results[78] show that functional groups able to form H-bonds to the P═O group significantly increase the heat of adsorption of DMMP. Detailed vibrational mode assignments for the IR and Raman spectra of liquid DMMP have been given by Moravie et al.[79]

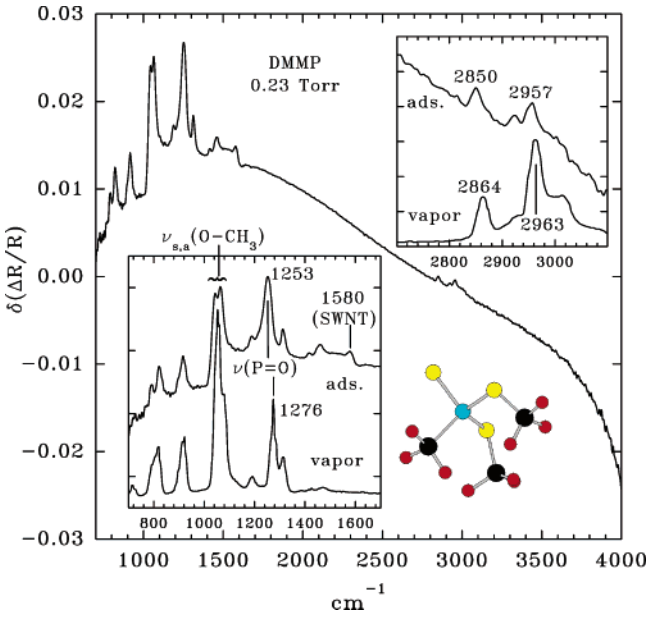

Figure 5. PM-IRRAS data for a SWNT/Al sample in a 0.23 Torr ambient of DMMP vapor. The transmission spectrum of DMMP vapor (ref 39) is also shown. The insets show parts of the spectrum in more detail, and various regions are assigned according to ref 79. "ν_s" and "ν_a" refer to symmetric and antisymmetric stretching modes. In the C−H stretching region (upper inset), adsorption-induced frequency shifts are noted in the more intense peaks. A schematic model of the DMMP molecular structure is also shown. In the lower inset, a feature believed to be due to the 1580 cm^{-1} SWNT phonon is indicated.

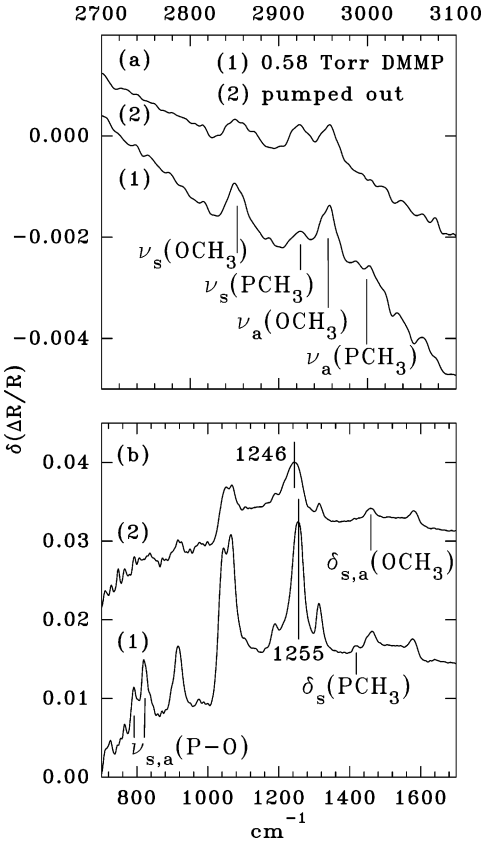

Figure 6. Similar to Figure 5 but showing the effects of evacuating a 0.58 Torr DMMP ambient. Note the different energy ranges in the two panels. Various regions are assigned according to ref 79. "δ_s" and "δ_a" refer to symmetric and antisymmetric C−H deformation modes. The two $-OCH_3$ deformations are too close in energy to resolve in the present data.

Figure 5 shows IR data for DMMP adsorbed on SWNTs and in the vapor phase.[39] The adsorbate spectrum was recorded in a 0.23 Torr ambient of DMMP vapor. The room-temperature vapor pressure[80] of DMMP is about 1.0 Torr. Due to the long (30 cm) optical path through the UHV chamber, strong absorptions occur due to gas-phase DMMP which are effectively eliminated in $\Delta R/R$. Except where noted, increasing the DMMP pressure to 0.58 Torr had no significant effect other than a uniform increase in the intensity of all bands. Because of the porous nature of the SWNT film, adsorbed DMMP molecules are randomly oriented with respect to the surface normal. Hence, all modes have a finite projection of the dynamic dipole moment on the surface normal and thus are detectable in PM-IRRAS. Except where noted below, all adsorbate peaks correspond to those observed for the molecular vapor, and none of the free-molecule peaks appear to be missing or strongly shifted in the adsorbate spectrum. This indicates that adsorption is nondissociative. However, small changes are noted in the positions and relative intensities of various peaks upon adsorption, and these effects will be discussed below.

A clear shift to lower energy is seen for the P═O stretching frequency of the adsorbate which indicates that this group is involved in bonding to the SWNT. The red-shift of ν(P═O) from the gas-phase value (1276 cm^{-1}) is known (e.g., refs 74 and 75) to be a sensitive indicator of the strength of the interaction between DMMP and the local environment. The data in Figure 5 show a shift of −23 cm^{-1} (to 1253 cm^{-1}) which is smaller than the shift of −34 cm^{-1} upon going from the vapor to the solid (ice) phase[74] of DMMP. These results are consistent with recent theoretical work[81] which finds that DMMP adsorption occurs via a very weak van der Waals interaction involving the P═O dipole.

An additional indication of the adsorbate structure is found in the $\nu_s(O-CH_3)$ and $\nu_a(O-CH_3)$ methoxy O−C stretching modes which give rise to the pair of overlapping peaks in the 1050−1075 cm^{-1} range. These are virtually unshifted from the vapor-phase energies, although there is a change in relative intensity. The lack of a significant frequency shift suggests that the O atoms in the $-OCH_3$ groups are *not* involved in bonding to the SWNT, unlike in the case of SiO_2 (ref 75) where they form H-bonds to surface −OH groups. In solid DMMP (ice), intermolecular interaction causes a −21 cm^{-1} shift[74] of $\nu_a(O-CH_3)$ and $\nu_s(O-CH_3)$, whereas, again, no similar shift is seen for adsorption on SWNTs.

As a check, similar experiments were performed for the bare Al reference substrate (see above). In a DMMP ambient of 0.23 Torr, very little adsorbate signal was detected. This consisted of weak, broad bands (not shown) at about 1050 and 1240 cm^{-1} in qualitative agreement with previous results[73] for exposure of Al_2O_3 powder to DMMP at room temperature. In the present case, the bare Al was not cleaned in situ other than by heating to about 520 °C in UHV and almost certainly was contaminated with amorphous C as well as with oxide. In any case, the results show that the spectra in Figures 5 and 6 receive no significant contribution from interaction between DMMP and the substrate.

There is one feature for DMMP adsorbed on SWNTs that does not appear in the vapor spectrum, namely, the peak at 1580 cm^{-1} indicated in Figure 5. This is close in energy to the SWNT >C═C< stretching mode (see above) and may indicate that this bond is perturbed by adsorption so as to increase the intensity (i.e., the dynamic dipole moment) of the mode without causing a significant shift in energy. An effect of this nature has been reported[82] in the ozonation of SWNTs. Another possible explanation lies in the observed (see below) reduction in free-carrier density that results from DMMP adsorption. This

would reduce the screening of the dynamic dipole moment of SWNT phonons and make such modes appear stronger in IRRAS.

Upon evacuation, part of the DMMP remains on the surface and subtle changes in the spectrum occur, as shown in Figure 6. The main effect of evacuating the DMMP is a uniform loss of intensity across the whole spectrum with slight changes in the relative intensities of various features (see below). However, ν(P═O) is further red-shifted (to 1246 cm^{-1}) and broadened somewhat, relative to the high-coverage spectrum, indicating that the remaining DMMP interacts more strongly with the SWNTs. A weaker interaction at higher coverage, corresponding to a higher P═O frequency, could result from a repulsive interaction between DMMP molecules due to steric effects. The shift could also indicate a distribution of different adsorption sites (due, e.g., to defects in the nanotube walls) such that the less attractive sites (with a higher P═O frequency) are populated only at higher coverage. The latter model, involving defect sites that saturate at lower coverage, is favored by the increased line width for the P═O mode after evacuation which suggests that such sites may be relatively more important at lower coverage.

Changes in the relative intensity of various features are noted in comparing the data in Figures 5 and 6. The sequence vapor → high coverage (0.58 Torr) → low coverage (pumped out) corresponds to an increase in the DMMP/SWNT interaction, as deduced from the trend in ν(P═O) discussed above. As the strength of the DMMP/SWNT interaction increases, the ν_s and ν_a modes for —OCH_3 maintain an approximately constant relative intensity, whereas $\nu_s(PCH_3)$ gains and $\nu_a(PCH_3)$ loses relative intensity. The $\delta_{a,s}(OCH_3)$ C—H deformation modes of the methoxy —CH_3, and perhaps the $\delta_s(PCH_3)$ C—H deformation of the —PCH_3, also gain relative intensity in the adsorbed state (Figure 5). The DMMP/SWNT interaction does not appear to affect other relative intensities, although ν_s(P—O) and ν_a(P—O) may be lost in the noise after evacuation (Figure 6b). Finally, small adsorption-induced shifts to lower energy are seen in the $\nu_s(OCH_3)$ and $\nu_a(OCH_3)$ modes (Figure 5).

Effects similar to those noted here have been seen[74] in comparing the transmission spectra of vapor-phase and condensed (ice) DMMP. This suggests that they are related to intermolecular interactions (in the case of DMMP ice) or to DMMP/SWNT interaction (in the present case). Due to the metal-surface IRRAS selection rule noted above, changes in dipole orientation with respect to the surface normal could also, in principle, affect relative intensities in the present experiments. However, such factors would not affect the DMMP ice data[74] which were obtained by transmission for an isotropic, nonmetallic substrate.

A further experiment was performed in which the SWNT sample was first exposed to H atoms, as described above, prior to exposing it to DMMP. This was done to determine if preadsorbed H would modify the DMMP/SWNT interaction to a measurable extent. The PM-IRRAS data (not shown) in a 0.23 Torr ambient of DMMP and after evacuation of the vapor were essentially identical to the corresponding results given above for a sample not previously exposed to H. This is consistent with the finding, noted above, that H adsorption under the present condition removes only a small fraction of the >C═C< sites.

A limited study of annealing effects (not shown) was also performed. After evacuation of the DMMP, heating to ~150 °C converted the spectrum to one resembling that reported[73] for DMMP on Al_2O_3, with almost complete elimination of the P═O stretching mode. This suggests that a mild thermal treatment causes desorption of DMMP from the SWNTs and/or diffusion from the SWNTs to the substrate. The further possibility of a reaction between DMMP and the SWNT at elevated temperature cannot, at present, be completely eliminated, especially in view of the results[77] for DMMP on activated carbon. However, the very weak DMMP/SWNT bonding at room temperature makes this appear to be unlikely.

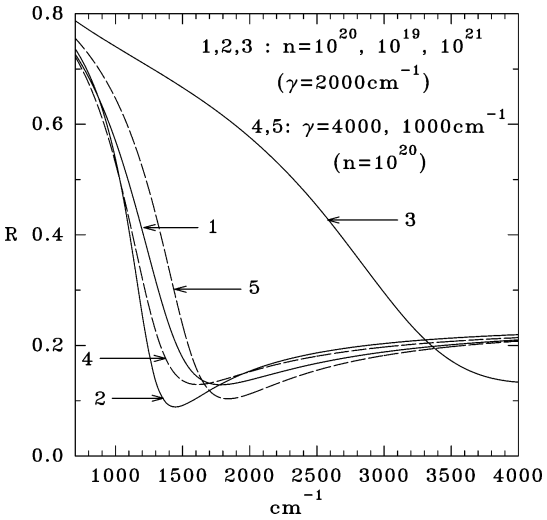

Figure 7. Normal-incidence reflectance, in air, for a semi-infinite SWNT substrate computed using a Drude—Lorentz dielectric function of the form given by Ugawa et al. (ref 86). The Drude parameters are $n = 1 \times 10^{20}$, 1×10^{19}, and 1×10^{21} cm^{-3}, respectively, for curves 1, 2, and 3 (all with $\gamma = 2000$ cm^{-1}). The corresponding plasmon frequencies are $\omega_p = 2994$, 947, and 9472 cm^{-1}, respectively. Curves 4 and 5, respectively, are for $\gamma = 4000$ and 1000 cm^{-1} (both with $n = 1 \times 10^{20}$ cm^{-3}).

3.4. The Broad Background. The DMMP spectra discussed above exhibit a broad and smoothly varying background that is completely reproducible. A similar phenomenon has been widely studied for metallic substrates (refs 83—85 and references therein), for which adsorption is seen to shift the background in the direction of decreasing R_p to a degree that increases with photon energy over the far- and mid-IR range. This has been explained quantitatively in terms of an adsorption-induced decrease in both the free-electron density at the surface (due to chemical bond formation) and the electron scattering lifetime. These effects are correlated with a measurable decrease in the electrical conductivity of metallic thin films when exposed to reactive gases. The net effect is to make the adsorbate-covered surface "look less metallic" in the IR than does the clean surface which leads to the observed decrease in R_p.

A similar discussion can be applied to the case of SWNTs using the Drude—Lorentz complex dielectric function introduced by Ugawa et al.[86] to account for the SWNT reflectance in the ~3 meV to 3 eV (~25 to 25 × 10^3 cm^{-1}) range. This is given by

$$\epsilon = (n + ik)^2 = \epsilon_\infty - \omega_p^2/(\omega^2 + i\gamma\omega) + \Sigma_j[\Omega_j^2/[(\omega_{0,j}^2 - \omega^2) - i\Gamma_j\omega] \quad (1)$$

where $\omega_p = (4\pi ne/m)^{1/2}$ is the plasmon frequency of the free-electron gas. Here, ω_p (cm^{-1}) = $(8.9698 \times 10^{-14}n)^{1/2}$ in terms of the carrier density n (cm^{-3}) and m and e are the carrier mass and charge (both set equal to the free-electron values). Figure 7 shows normal-incidence reflectance spectra calculated using eq 1 and the Fresnel relations for a semi-infinite SWNT substrate in air with different values for n and γ (the plasmon damping term). These results are useful in visualizing the relationship

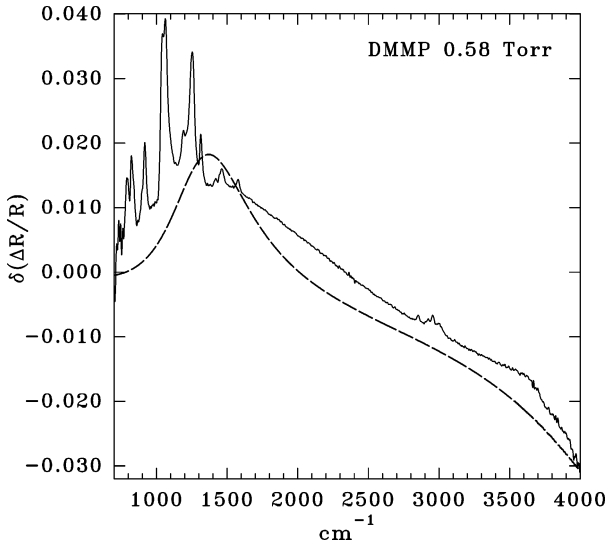

Figure 8. (solid) PM-IRRAS data for a SWNT sample in a DMMP ambient of 0.58 Torr. (dashed) Computed spectrum for a SWNT layer on Al showing the effect of modification of the Drude parameters by DMMP adsorption (see text).

between the electronic and mid-IR optical properties. The single-oscillator Lorentz parameters ($\Omega = 3629$ cm^{-1}, $\omega_0 = 161.3$ cm^{-1}, $\Gamma = 338.7$ cm^{-1}) and the frequency-independent term ($\epsilon_\infty = 8.5$) are those given in ref 86 for room temperature. The conduction in air-exposed SWNTs occurs via holes;[8,52] however, no distinction is made here between holes and electrons as the majority carriers. Curve 1 in Figure 7, with $n = 1 \times 10^{20}$ cm^{-3} and $\gamma = 2000$ cm^{-1}, corresponds approximately to the single-oscillator best-fit results discussed by Ugawa et al. for their sample.[86]

Figure 7 illustrates the basic points mentioned above. Increasing n or decreasing γ ($=1/\tau$, where τ is the electron scattering lifetime) makes the substrate "look more metallic", leading to an increased reflectance. Note that the differences between the curves in Figure 7 are much greater than the adsorbate-induced reflectance changes seen in the data given above. Hence, $\delta(\Delta R/R)$ is expected to be very sensitive to changes in the Drude parameters. Any adsorbate is expected to increase γ, but the SWNT n can change in either direction depending on the chemical species. The situation is further complicated, in the case of SWNTs, by the combined presence of both Drude and Lorentz terms. It is noted that a similar approach has been applied to a qualitative interpretation of changes in the IR diffuse reflectance spectra of SWNTs following saturation with H_2 at high pressure.[87]

Figure 8 shows the application of this model to DMMP adsorption on SWNTs. The calculation was done for a SWNT layer on Al (ignoring any chemical effects at the interface) at an angle of incidence of 82° as in the experiment. The single-oscillator Drude−Lorentz function described above was used to model the SWNT layer, ignoring any anisotropy in the optical constants, and the Al optical constants were obtained from tabulated data.[88] An effective SWNT layer thickness of 50 nm was assumed, and the Drude parameters for both the bare and DMMP-covered SWNT layer were varied by trial and error in order to reproduce qualitatively the overall shape of the background. The adsorbate was assumed to affect the entire depth of the SWNT layer uniformly. The calculated spectrum was very sensitive to all four parameters, that is, n and γ before and after DMMP adsorption, and the result shown in Figure 8 was divided by a factor of 5 in order to match the scale of the observed spectrum.

The computed spectrum in Figure 8 was obtained with $n = 2 \times 10^{21}$ (2×10^{20}) cm^{-3} and $\gamma = 2 \times 10^3$ (6×10^3) cm^{-1} before (after) DMMP adsorption. The results show that the simple and approximate model used here can account qualitatively for the overall shape of the background. The sample is assumed to be a mixture of metallic and semiconducting tubes, and the n values thus represent average quantities. The adsorbate-induced changes in n and γ are both consistent with the observed[34] increase in resistance when a SWNT layer is exposed to DMMP. In principle, a more accurate least-squares fitting procedure should enable the determination of SWNT electronic properties from IR reflectance data. The effect of adsorbed H was not considered, since it alters the structure of the SWNT wall, as discussed above, which means that the optical effects of H cannot be modeled simply in terms of changes in the Drude parameters. Furthermore, H adsorption under the present conditions appears to occur locally, rather than uniformly over the entire SWNT, which would lead to an inhomogeneous H/SWNT layer.

4. Summary

Carbon nanotubes were deposited on an Al substrate and cleaned by heating in UHV. The sample was then exposed to H (or D) atoms and/or to DMMP, and PM-IRRAS spectra were recorded. The results are as follows.

(1) The PM-IRRAS approach is shown to be a viable technique for obtaining vibrational spectroscopic data for adsorption on SWNTs deposited on metallic substrates. It is thus possible to observe weakly interacting surface species under finite steady-state reagent pressures. Although the present work has focused entirely on IR-spectroscopic aspects, the use of a metallic substrate[15] will also facilitate the application of surface-sensitive electron spectroscopies such as AES and XPS.

(2) Adsorption of atomic H occurs preferentially near strained or defective regions in the nanotube wall to produce a spectrum consistent with alkane-like species ($>CH_2$ and $-CH_3$). Only a small fraction of the $>C{=}C<$ sites in the nanotube wall react with H, and there is no clear indication for production of monohydride $>C(H)-C(H)<$ species.

(3) For DMMP, data were obtained under steady-state conditions in reagent pressures in excess of half the room-temperature vapor pressure. Adsorption occurs via the P═O group with a coverage that depends on the ambient pressure. Varying the DMMP coverage by changing the ambient pressure causes changes in the spectrum that can be related to the strength of the DMMP/SWNT interaction. Preadsorbed H is seen to have little or no effect on the subsequent adsorption of DMMP.

(4) The DMMP molecular features are superimposed on a broad, smoothly varying background that can be related to adsorption-induced changes in the Drude parameters characterizing the SWNT free-carrier density and scattering lifetime.

A shortcoming of the present approach, and of any others involving SWNTs supported on another material, is the issue of substrate effects. The data presented here show only minor features due to adsorption on the support, such as AlOD formation during D-atom exposure and reaction with DMMP during annealing. However, similar experiments with NO_2 (not discussed here) were in fact dominated by adsorption on the oxidized Al surface. In principle, such perturbations could be diminished through the use of a more inert material such as Au, but the possibility of substrate effects, which have been documented here, remains a concern. A further issue has to do with chemical reaction between the SWNTs and the substrate, particularly for high-temperature anneals when the support is a

carbide-forming metal. Some indication of such an effect has been seen here in the formation of Al−O−C bonds during annealing. This ability to detect chemical processes at the SWNT/metal interface actually offers certain opportunities. Recent work[89] has shown that the electronic properties of SWNT/metal contacts can be significantly modified by the introduction of organic adsorbates, and it thus appears feasible to study such phenomena spectroscopically. In principle, the ability to perform AES or XPS measurements in parallel with the IR experiments will shed light on the issue of substrate effects.

Acknowledgment. This work was supported by the Office of Naval Research. S. C. Badescu is thanked for helpful discussions on the theory of molecular adsorption on SWNTs. L. Ericson is thanked for preparing the SWNT film samples and for advice on sample preparation. J. P. Long is thanked for providing the D_2 gas. J. C. Owrutsky is thanked for pointing out ref 86. F. K. Perkins is thanked for help in writing the MS Excel macro for applying the $J_0(A)$ correction. J. N. Russell, Jr., is thanked for electrolytically polishing the Al substrates and for making the W filament assembly used for H_2 dissociation.

References and Notes

(1) Lin, Y.; Taylor, S.; Li, H.; Shiral Fernando, K. A.; Qu, L.; Wang, W.; Gu, L.; Zhou, B.; Sun, Y.-P. *J. Mater. Chem.* **2004**, *14*, 527.
(2) Dyke, C. A.; Tour, J. M. *J. Phys. Chem. A* **2004**, *108*, 11151.
(3) Banerjee, S.; Hemraj-Benny, T.; Wong, S. S. *Adv. Mater.* **2005**, *17*, 17.
(4) Goldoni, A.; Larciprete, R.; Petaccia, L.; Lizzit, S. *J. Am. Chem. Soc.* **2003**, *125*, 11329.
(5) Kim, W.; Javey, A.; Vermesh, O.; Wang, Q.; Li, Y.; Dai, H. *Nano Lett.* **2003**, *3*, 193.
(6) Zahab, A.; Spina, L.; Poncharal, P.; Marlière, C. *Phys. Rev. B* **2000**, *62*, 10000.
(7) Dean, K. A.; Chalamala, B. R. *Appl. Phys. Lett.* **1999**, *75*, 3017.
(8) Collins, P. G.; Bradley, K.; Ishigami, M.; Zettl, A. *Science* **2000**, *287*, 1801.
(9) Bermudez, V. M. *Appl. Surf. Sci.* **2000**, *161*, 227.
(10) Knotek, M. L.; Houston, J. E. *J. Vac. Sci. Technol.* **1982**, *20*, 544.
(11) Hennrich, F.; Lebedkin, S.; Malik, S.; Tracy, J.; Barczewski, M.; Rösner, H.; Kappes, M. *Phys. Chem. Chem. Phys.* **2002**, *4*, 2273.
(12) Ellison, M. D.; Crotty, M. J.; Koh, D.; Spray, R. L.; Tate, K. E. *J. Phys. Chem. B* **2004**, *108*, 7938.
(13) Feng, X.; Matranga, C.; Vidic, R.; Borguet, E. *J. Phys. Chem. B* **2004**, *108*, 19949.
(14) Hunt, M. R. C.; Montalti, M.; Chao, Y.; Krishnamurthy, S.; Dhanak, V. R.; Šiller, L. *Appl. Phys. Lett.* **2002**, *81*, 4847.
(15) Kuznetsova, A.; Yates, J. T., Jr.; Liu, J.; Smalley, R. E. *J. Chem. Phys.* **2000**, *112*, 9590.
(16) Bermudez, V. M. *J. Vac. Sci. Technol., A* **1992**, *10*, 152.
(17) Gardner, P.; LeVent, S.; Pilling, M. J. *Surf. Sci.* **2004**, *559*, 186.
(18) Chabal, Y. J. *Surf. Sci. Rep.* **1988**, *8*, 211.
(19) Bermudez, V. M.; Prokes, S. M. *Surf. Sci.* **1991**, *248*, 201.
(20) Ehrley, W.; Butz, R.; Mantl, S. *Surf. Sci.* **1991**, *248*, 193.
(21) Pilling, M. J.; Gardner, P.; Pemble, M. E.; Surman, M. *Surf. Sci.* **1998**, *418*, L1.
(22) Paulidou, A.; Nix, R. M. *Surf. Sci.* **2000**, *470*, L104.
(23) Noda, H.; Urisu, T.; Kobayashi, Y.; Ogino, T. *Jpn. J. Appl. Phys.* **2000**, *39*, 6985.
(24) Eng, J., Jr.; Raghavachari, K.; Struck, L. M.; Chabal, Y. J.; Bent, B. E.; Flynn, G. W.; Christman, S. B.; Chaban, E. E.; Williams, G. P.; Radermacher, K.; Mantl, S. *J. Chem. Phys.* **1997**, *106*, 9889.
(25) Beitel, G. A.; Laskov, A.; Oosterbeek, H.; Kuipers, E. W. *J. Phys. Chem.* **1996**, *100*, 12494. Beitel, G. A.; de Groot, C. P. M.; Oosterbeek, H.; Wilson, J. H. *J. Phys. Chem. B* **1997**, *101*, 4035.
(26) Bermudez, V. M. *J. Vac. Sci. Technol., A* **1998**, *16*, 2572.
(27) Bermudez, V. M. *Thin Solid Films* **1999**, *347*, 195. Bermudez, V. M.; DeSisto, W. J. *J. Vac. Sci. Technol., A* **2001**, *19*, 576.
(28) Stacchiola, D.; Thompson, A. W.; Kaltchev, M.; Tysoe, W. T. *J. Vac. Sci. Technol., A* **2002**, *20*, 2101.
(29) Ozensoy, E.; Hess, C.; Goodman, D. W. *J. Am. Chem. Soc.* **2002**, *124*, 8524.
(30) Kim, K. S.; Bae, D. J.; Kim, J. R.; Park, K. A.; Lim, S. C.; Kim, J.-J.; Choi, W. B.; Park, C. Y.; Lee, Y. H. *Adv. Mater.* **2002**, *14*, 1818.
(31) Barone, V.; Heyd, J.; Scuseria, G. E. *J. Chem. Phys.* **2004**, *120*, 7169.
(32) Gülseren, O.; Yildirim, T.; Ciraci, S. *Phys. Rev. B* **2002**, *66*, 121401-(R).
(33) Sieber, N.; Mantel, B. F.; Seyller, Th.; Ristein, J.; Ley, L. *Diamond Relat. Mater.* **2001**, *10*, 1291.
(34) Novak, J. P.; Snow, E. S.; Houser, E. J.; Park, D.; Stepnowski, J. L.; McGill, R. A. *Appl. Phys. Lett.* **2003**, *83*, 4026.
(35) Chase, D. B. *Appl. Spectrosc.* **1984**, *38*, 491.
(36) Carter, R. O., III; Lindsay, N. E.; Beduhn, D. *Appl. Spectrosc.* **1990**, *44*, 1147.
(37) Kuzumaki, T.; Miyazawa, K.; Ichinose, H.; Ito, K. *J. Mater. Res.* **1998**, *13*, 2445.
(38) Sutoh, A.; Okada, Y.; Ohta, S.; Kawabe, M. *Jpn. J. Appl. Phys.* **1995**, *34*, L1379.
(39) National Institute of Standards and Technology Chemistry WebBook (http://webbook.nist.gov/chemistry).
(40) Kuznetsova, A.; Mawhinney, D. B.; Naumenko, V.; Yates, J. T., Jr.; Liu, J.; Smalley, R. E. *Chem. Phys. Lett.* **2000**, *321*, 292.
(41) Matranga, C.; Chen, L.; Smith, M.; Bittner, E.; Johnson, J. K.; Bockrath, B. *J. Phys. Chem. B* **2003**, *107*, 12930.
(42) Gromovoy, T. Yu.; Palyanytsya, B. B.; Pokrovskiy, V. A.; Basiuk, E. V.; Basiuk, V. A. *J. Nanosci. Nanotechnol.* **2004**, *4*, 77.
(43) Murakami, Y.; Einarsson, E.; Edamura, T.; Maruyama, S. *Phys. Rev. Lett.* **2005**, *94*, 087402.
(44) Kuhlmann, U.; Jantoljak, H.; Pfänder, N.; Bernier, P.; Journet, C.; Thomsen, C. *Chem. Phys. Lett.* **1998**, *294*, 237.
(45) Kuzmany, H.; Burger, B.; Thess, A.; Smalley, R. E. *Carbon* **1998**, *36*, 709.
(46) van den Brink, R. W.; Mulder, P.; Louw, R.; Sinquin, G.; Petit, C.; Hindermann, J.-P. *J. Catal.* **1998**, *180*, 153.
(47) Brüesch, P.; Kötz, R.; Neff, H.; Pietronero, L. *Phys. Rev. B* **1984**, *29*, 4691.
(48) Kouklin, N.; Tzolov, M.; Straus, D.; Yin, A.; Xu, J. M. *Appl. Phys. Lett.* **2004**, *85*, 4463.
(49) Williams, K. A.; Pradhan, B. K.; Eklund, P. C.; Kostov, M. K.; Cole, M. W. *Phys. Rev. Lett.* **2002**, *88*, 165502.
(50) Lin, J.-C.; Chen, K.-H.; Chang, H.-C.; Tsai, C.-S.; Lin, C.-E.; Wang, J.-K. *J. Chem. Phys.* **1996**, *105*, 3975.
(51) Dillon, A. C.; Yudasaka, M.; Dresselhaus, M. S. *J. Nanosci. Nanotechnol.* **2004**, *4*, 691.
(52) Valentini, L.; Armentano, I.; Puglia, D.; Lozzi, L.; Santucci, S.; Kenny, J. M. *Thin Solid Films* **2004**, *449*, 105.
(53) Zhang, L.; Kiny, V. U.; Peng, H.; Zhu, J.; Lobo, R. F. M.; Margrave, J. L.; Khabashesku, V. N. *Chem. Mater.* **2004**, *16*, 2055.
(54) Osswald, S.; Flahaut, E.; Ye, H.; Gogotsi, Y. *Chem. Phys. Lett.* **2005**, *402*, 422.
(55) Srivastava, D.; Brenner, D. W.; Schall, J. D.; Ausman, K. D.; Yu, M.; Ruoff, R. S. *J. Phys. Chem. B* **1999**, *103*, 4330.
(56) Astakhova, T. Yu.; Vinogradov, G. A.; Gurin, O. D.; Menon, M. *Izv. Akad. Nauk., Ser. Khim.* **2002**, 704; *Russ. Chem. Bull., Int. Ed.* **2002**, *51*, 764 (English translation).
(57) Okuyama, H.; Thachepan, S.; Aruga, T.; Ando, T.; Nishijima M. *Chem. Phys. Lett.* **2003**, *381*, 535.
(58) King, G. W. *Spectroscopy and Molecular Structure*; Holt, Rinehart and Winston: New York, 1964.
(59) Ley, L.; Mantel, B. F.; Matura, K.; Stammler, M.; Janischowsky, K.; Ristein, J. *Surf. Sci.* **1999**, *427−428*, 245.
(60) MacPhail, R. A.; Strauss, H. L.; Snyder, R. G.; Elliger, C. A. *J. Phys. Chem.* **1984**, *88*, 334.
(61) Crowell, J. E.; Chen, J. G.; Hercules, D. M.; Yates, J. T., Jr. *J. Chem. Phys.* **1987**, *86*, 5804.
(62) Frederick, B. G.; Apai, G.; Rhodin, T. N. *Surf. Sci.* **1991**, *244*, 67.
(63) Bauschlicher, C. W., Jr.; So, C. R. *Nano Lett.* **2002**, *2*, 337. Bauschlicher, C. W., Jr. *Nano Lett.* **2001**, *1*, 223.
(64) Arellano, J. S.; Molina, L. M.; Rubio, A.; López, M. J.; Alonso, J. A. *J. Chem. Phys.* **2002**, *117*, 2281.
(65) Volpe, M.; Cleri, F. *Surf. Sci.* **2003**, *544*, 24.
(66) Peng, S.; Cho, K. *Nanotechnology* **2000**, *11*, 57.
(67) Mantel, B. F.; Stammler, M.; Ristein, J.; Ley, L. *Diamond Relat. Mater.* **2001**, *10*, 429.
(68) Porter, M. D.; Bright, T. B.; Allara, D. L.; Chidsey, C. E. D. *J. Am. Chem. Soc.* **1987**, *109*, 3559.
(69) Jung, Y. S.; Jeon, D. Y. *Appl. Surf. Sci.* **2002**, *193*, 129.
(70) Tsai, S. H.; Chiang, F. K.; Tsai, T. G.; Shieu, F. S.; Shih, H. C. *Thin Solid Films* **2000**, *366*, 11.
(71) Li, Y.-X.; Schlup, J. R.; Klabunde, K. J. *Langmuir* **1991**, *7*, 1394.
(72) Aurian-Blajeni, B.; Boucher, M. M. *Langmuir* **1989**, *5*, 170.
(73) Mitchell, M. B.; Sheinker, V. N.; Mintz, E. A. *J. Phys. Chem. B* **1997**, *101*, 11192.
(74) Rusu, C. N.; Yates, J. T., Jr. *J. Phys. Chem. B* **2000**, *104*, 12292.
(75) Kanan, S. M.; Tripp, C. P. *Langmuir* **2001**, *17*, 2213.

(76) Zhou, J.; Varazo, K.; Reddic, J. E.; Myrick, M. L.; Chen, D. A. *Anal. Chim. Acta* **2003**, *496*, 289.
(77) Cao, L.; Suib, S. L.; Tang, X.; Satyapal, S. *J. Catal.* **2001**, *197*, 236.
(78) Bertilsson, L.; Engquist, I.; Liedberg, B. *J. Phys. Chem. B* **1997**, *101*, 6021. Bertilsson, L.; Potje-Kamloth, K.; Liess, H.-D.; Liedberg, B. *Langmuir* **1999**, *15*, 1128.
(79) Moravie, R. M.; Froment, F.; Corset, J. *Spectrochim. Acta* **1989**, *45A*, 1015.
(80) Tevault, D. E.; Buchanan, J. H.; Buettner, L. C. Proceedings of the 15th Symposium on Thermophysical Properties; National Institute of Standards and Technology: Boulder, CO, 2003; p 440 (available online at http://symp15.nist.gov/pdf/p440.pdf).
(81) Badescu, S. C.; Reineke, T. L. Manuscript to be published.
(82) Cai, L.; Bahr, J. L.; Yao, Y.; Tour, J. M. *Chem. Mater.* **2002**, *14*, 4235.
(83) Tobin, R. G. *Surf. Sci.* **2002**, *502*−*503*, 374.
(84) Fahsold, G.; Sinther, M.; Priebe, A.; Diez, S.; Pucci, A. *Phys. Rev. B* **2002**, *65*, 235408.
(85) Hein, M.; Dumas, P.; Otto, A.; Williams, G. P. *Surf. Sci.* **1999**, *419*, 308.
(86) Ugawa, A.; Hwang, J.; Gommans, H. H.; Tashiro, H.; Rinzler, A. G.; Tanner, D. B. *Curr. Appl. Phys.* **2001**, *1*, 45. Ugawa, A.; Rinzler, A. G.; Tanner, D. B. *Phys. Rev. B* **1999**, *60*, R11305.
(87) Bashkin, I. O.; Antonov, V. E.; Bazhenov, A. V.; Bdikin, I. K.; Borisenko, D. N.; Krinichnaya, E. P.; Moravsky, A. P.; Harkunov, A. I.; Shul'ga, Yu. M.; Ossipyan, Yu. A.; Ponyatovsky, E. G. *Pis'ma Zh. Eksp. Teor. Fiz.* **2004**, *79*, 280; *JETP Lett.* **2004**, *79*, 226 (English translation).
(88) Smith, D. Y.; Shiles, E.; Inokuti, M. In *Handbook of Optical Constants of Solids*; Palik, E. D., Ed.; Academic: Orlando, FL, 1985.
(89) Auvray, S.; Borghetti, J.; Goffman, M. F.; Filoramo, A.; Derycke, V.; Bourgoin, J. P.; Jost, O. *Appl. Phys. Lett.* **2004**, *84*, 5106.